Li et al., 2018, Connections between subducted sediment, pore-fluid pressure, and earthquake behavior along the Alaska megathrust: Geology, https://doi.org/10.1130/G39557.1.

SUPPLEMENTARY MATERIAL

Prestack Depth Migration and Uncertainty Analysis

Three MCS profiles collected during the ALEUT project (Fig. 1) are analyzed in this work via 2D Kirchoff PSDM approach to produce detailed velocity models and reflection images (Figs. S1, S2). The initial velocity model was based on a combination smoothed RMS velocities converted into depth in the sediments and smoothed first-arrival travel-time tomography from OBS data in the crust (Shillington et al., 2015). Residual velocity analysis based on depth-migrated common reflection point (CRP) gathers was used to update and improve the velocity model. Several iterations of PSDM were performed to refine the velocity model until reflections in the CRP gathers were flattened.

To assess the uncertainty of the final velocity models, we first perturbed all velocities by ± 5% and ± 10%, and qualitatively assessed the flatness of key reflections in the resulting CRP gathers (Fig. S3). From this analysis, the overall velocity model has an uncertainty of ~5%. On Lines 3 and 4, where we clearly observed two parallel reflection bands representing the top and base of the subducted sediment channel, a low velocity zone (LVZ) is required in this interval to flatten the deeper reflection. We removed the low-velocity zone from both velocity models, and the resulting common reflection point gathers clearly show that the lower reflection from this boundary is not flat (Fig. S4). On Line 5, the subducted sediment channel is also characterized by a LVZ, which is however thin, rugged and disappears quickly landward.

We further analyzed the uncertainty of the velocities determined by PSDM by perturbing the velocity within the subducted sediment layer in our final models for each line by ± 5%, ± 10%, and ± 20%. We then checked the flatness of the lower reflections from the base of the LVZ on every ~50 to 100th migrated CRP gather after re-running PSDM with the perturbed velocity models. In general, the velocity uncertainties within the subduction channel increase as the sediments are subducted to greater depths. From examining the locations where two parallel reflections are visible, we obtained the following estimations of the velocity uncertainties: 1) Line 3, 5% to 10% to 20% at locations 5 km, 15 km and 25 km from the trench, respectively (Fig. S5); 2) Line 4, 5% to 10% at locations 10 km and 15 km from the trench (Fig. S6); 3) Line 5, 5% to 10% to 15% at locations 2.5 km, 5 km and 10 km from the trench (Fig. S7). On Line 3, at depths greater than ~8–

10 km in depth, we can still image a subducted sediment layer along megathrust fault, but the aperture is inadequate to constrain the velocities within this layer.

The velocity model for Line 4 exhibits a sharp landward change in velocity of the overriding plate. Although this velocity model appears to best explain the reflections in overriding plate used in velocity analysis, we are not confident in this feature and thus do not interpret it. This anomalous velocity change occurs landward of the underlying LVZ, and thus does not impact the analysis presented in this paper based on velocities, which if focused within 15 km of the trench (Figs. 2b, S1).

We also wish to point out that the PSDM analysis presented in this paper depends on identifying independent reflections from the top and base of a layer to constrain velocities within it. As a result, we cannot constrain the properties of very thin (<50 m thick) layers along the plate boundary. For example, a thin LVZ could lie along the Shumagin megathrust landward of the small LVZ described in the main text, and it would not be resolved by our analysis.

Pore-fluid pressure estimation

The observed velocities from the PSDM are compared with predicted velocities for different pore-fluid pressure conditions to estimate *in situ* pore-fluid pressure variations in the Alaska subduction zone. Predicted velocities for a suite of pore-fluid pressure conditions are determined using the following steps:

1) We compute the *in situ* porosity (ϕ) from the PSDM velocities for a series of vertical profiles on the incoming plate at the three transects using a relation between porosity and Vp established for marine mudstones offshore the Nankai Trough (Hoffman & Tobin, 2004). This relationship also provides an excellent fit to available data from the Alaska margin from DSDP Legs 18 and 19 (open blue and green symbols in Fig. S8a).

2) The estimated porosity values are used to estimate bulk density assuming a grain density of 2.7 g/cm^3, and density is used to compute the vertical effective stress (σ_v') as a function of depth on

the incoming plate. We assume hydrostatic pore-fluid pressure for these slowly deposited sediments on the incoming oceanic plate (Hart et al., 1995; Saffer, 2003; Tobin and Saffer, 2009) .

3) Using the porosities and effective stresses estimated above, we then establish a relationship between effective stress and void ratio (*e*) (hereafter called the compression trend), where *e* is related to porosity by:

$$e = \frac{\phi}{1-\phi}$$

We find a log-linear trend of decreasing void ratio with vertical effective stress. This is a typical behavior for soils and sediments (Saffer, 2003; Tobin and Saffer, 2009), and the trend is well described by the relation: e = 0.78 - 0.385 log(σ_v') (Fig. S8b).

4) We then use this compression trend in a series of forward models designed to explore the predicted compression state and P-wave velocity of the sediment layer for a range of presumed pore pressure ratios (λ^*). We predict the *in situ* void ratio (and thus porosity) as a function of distance landward of the trench along each seismic line, using the total overburden stress at the midpoint of the subducted layer, and for a range of presumed pore pressure ratios (λ^* = 0, 0.2, 0.4, 0.6, and 0.8), following the approach of Tobin & Saffer (2009) and Calahorrano et al. (2008).

5) Finally, the predicted Vp associated with the porosity is estimated at each location from the relation of Hoffman & Tobin (2004) (Fig. S8a). This yields a series of predicted Vp values within the subducting layer for comparison with the observed Vp from PSDM (Fig. 3).

We assume uniaxial compression in all of the calculations above, a simplified approach widely used in previous studies [Calahorrano et al., 2008; Tobin and Saffer, 2009; Bassett et al., 2014], and defensible on the basis of field studies [e.g., Byrne and Fisher, 1990] and drilling [e.g., Saffer, 2003]. In reality, the stress state is likely to be somewhat more complicated because shear stress may be transmitted across the plate interface to the subducting sediments [e.g., Bangs et al., 1990; Hayward et al., 2003]. In this context, our assumption of uniaxial burial provides a lower

bound on pore pressure estimation, and thus constitutes a conservative estimate [Kitajima and Saffer, 2012].

There is some scatter in the relationships between velocity and porosity, porosity and density, and void ratio and vertical effective stress that are used to calculated predicted Vp for different pore-fluid pressure conditions. Although this scatter leads to uncertainty in the absolute values of pore-fluid pressures estimated for each profile, it does not change the relative variations in estimated pore-fluid pressure along the margin, which are the basis for our interpretation.

Figure S1: Prestack depth migrations of ALEUT Lines 3-5 overlain on velocity models determined from PSDM. Red lines show locations of CRP gathers shown in Figs. S2-S6.

Figure S2: Prestack depth migrations of ALEUT Lines 3-5 without interpretations or velocity in the background.

Figure S3: Example of CRP gathers from each line showing impact of perturbing entire velocity model by -10%, -5%, 0, +5%, +10%. a) Line 3, CRP 36566; b) Line 4, CRP 22602, c) Line 5, CRP 26660.

Figure S4. Example of CRPs with final velocity model (left) and with low-velocity zone (LVZ) within sediment channel removed (right). Note that the reflection from the base of the channel (indicated with red arrow) is clearly not flattened without the LVZ. The depth of this reflection changes between the two CRPs because of the change in the velocity model. a) CRP 36566, Line 3; b) CRP 22700, Line 4. See Fig. S1 for locations of CRPs.

Figure S5. Examples of CRPs from Line 3 with perturbed velocities within the subducting sediment channel (indicated with red arrows) of -20%, -10%, -5%, 0%, +5%, +10%, +20%, from left to right. a) CRP 38806, b) CRP 36569. See Fig. S1 for locations of CRPs.

Figure S6. Examples of CRPs from Line 4 with perturbed velocities within the sediment channel (indicated with red arrows) of -20%, -10%, -5%, 0%, +5%, +10%, +20%, from left to right. a) CRP 22666, b) CRP 23862. See Fig. S1 for locations of CRPs.

Figure S7. Examples of CRPs from Line 5 with perturbed velocities within the sediment channel of -20%, -10%, 5%, 0%, +5%, +10%, +20%. a) CRP 27855, b) CRP 27258. See Fig. S1 for locations of CRPs.

Figure S8. a) Relation between compressional wave velocity and porosity for fine-grained hemipelagic and pelagic sediments collected at DSDP Sites 178 (dark blue circles), 183 (light blue), and 186 (green) offshore Alaska, and from high-stress (70-90 MPa) laboratory experiments on samples of exhumed subducted sediments from Kodiak Island (Miller et al., 2016). Data from the Nankai Trough are shown for comparison, including laboratory measurements from Kitajima & Saffer (2012)(filled grey circles) and Tsuji et al. (2005)(open black circles), and from drilling at IODP Site C0011 (crosses). The relation of Hoffman & Tobin (2004) used in our analysis is also shown. b) Compression trend defined between void ratio (e) and vertical effective stress (σ_v') for incoming sediments along the three transects. The black dashed line shows the empirical relationship fit to the observations.

References

Calahorrano, A., Sallares, V., Collot, J.-Y., Sage, F., and Ranero, C. R., 2008, Nonlinear variations of the physical properties along the southern Ecuador subduction channel: Results from depth-migrated seismic data: Earth Planet. Sci. Lett., v. 267, p. 453-467.

Hart, B. S., Flemings, P. B., and Deshpande, A., 1995, Porosity and pressure - role of compaction disequilibrium in the development of geopressures in a gulf-coast pleistocene basin: Geology, v. 23, p. 45-48.

Hoffman, N. W., and Tobin, H. J., 2004, 11. An Empiral Relationship between Velocity and Porosity for Underthrust Sediments in the Nankai Trough Accretionary Prism, *in* Mikada, H., Moore, G. F., Taira, A., Becker, K., Moore, J. C., and Klaus, A., eds., Proc. ODP Sci. Results. 190/196, Ocean Drilling Program, p. 1-23.

Kitajima, K., and Saffer, D. M., 2012, Elevated pore pressure and anomalously low stress in regions of low frequency earthquakes along the Nankai Trough subduction megathrust: Geophys. Res. Lett., v. 39, p. L23301, doi:23310.21029/22012GL053793.

Miller, P., Abers, G. A., Saffer, D. M., Bate, C., Shillington, D. J., Keranen, K. M., Bécel, A., and Li, J., 2016, Anisotropy in P and S-wave velocities in exhumed metasediments from the Aleutian Megathrust: Implications for the interpretation of low velocity zones: Eos, Transactions, AGU Fall Meeting.

Saffer, D. M., 2003, Pore pressure development and progressive dewatering in underthrust sediments at the Costa Rican subduction margin: Comparison with northern Barbados and Nankai: Journal of Geophysical Research-Solid Earth, v. 108, no. B5.

Shillington, D. J., Bécel, A., Nedimović, M. R., Kuehn, H., Webb, S. C., Abers, G. A., Keranen, K. M., Li, J., Delescluse, M., and Mattei-Salicrup, G. A., 2015, Link between plate fabric, hydration and subduction zone seismicity in Alaska: Nature Geoscience, v. 8, p. 961-964, doi:910.1038/ngeo2586.

Tobin, H. J., and Saffer, D. M., 2009, Elevated fluid pressure and extreme mechanical weakness of a plate boundary thrust, Nankai Trough subduction zone: Geology, v. 37, no. 8, p. 679-682.

Tsuji, T., Matsuoka, T., Yamada, Y., Nakamura, Y., Ashi, J., Tokuyama, H., Kuramoto, S., and Bangs, N. L., 2005, Initiation of plate boundary slip in the Nankai Trough off the Muroto peninsula, southwest Japan: Geophys. Res. Lett., v. 32, no. 12, p. L12306, doi:12310.11029/12004GL021861.

Figure S1, Li et al

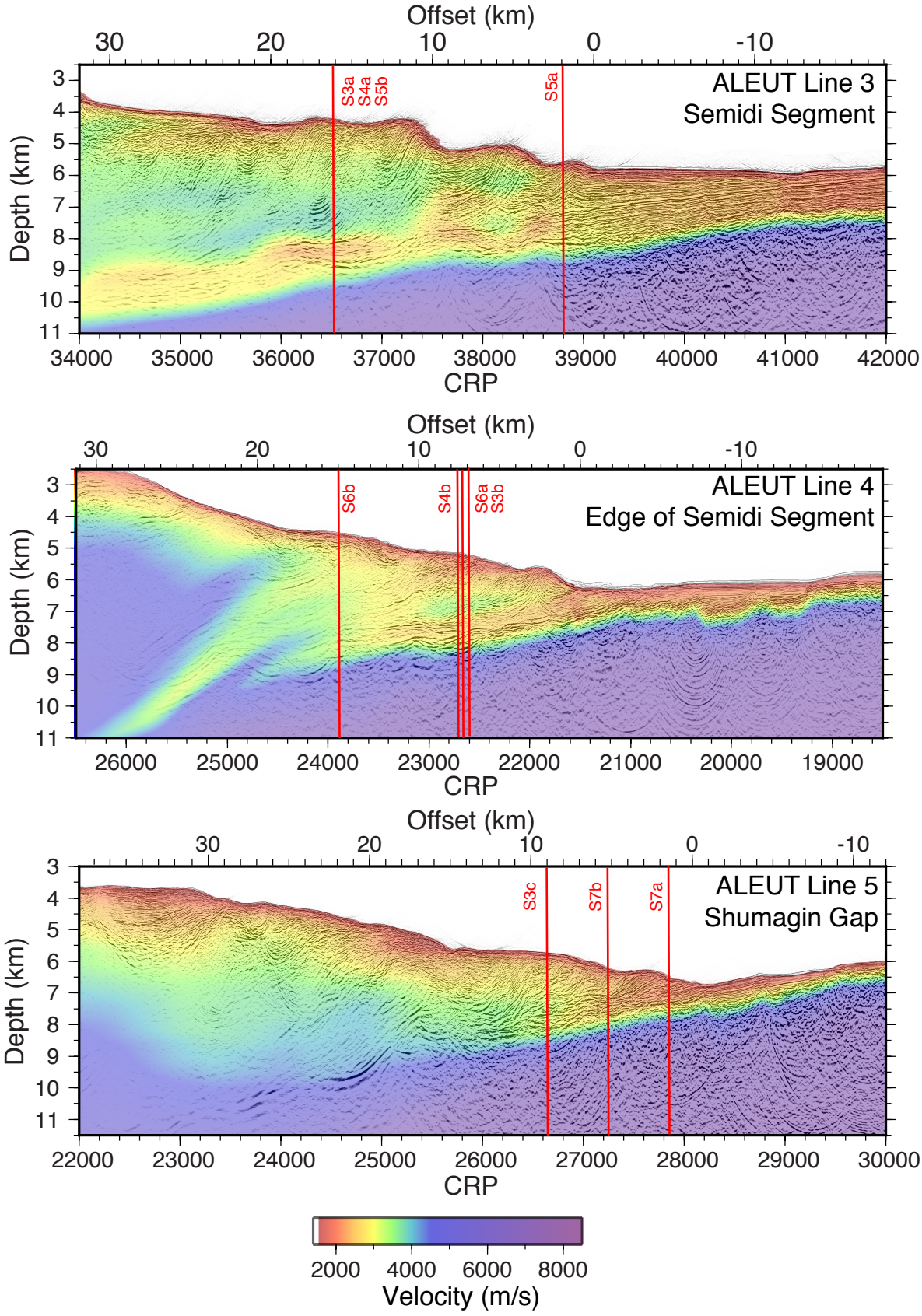

Figure S2, Li et al

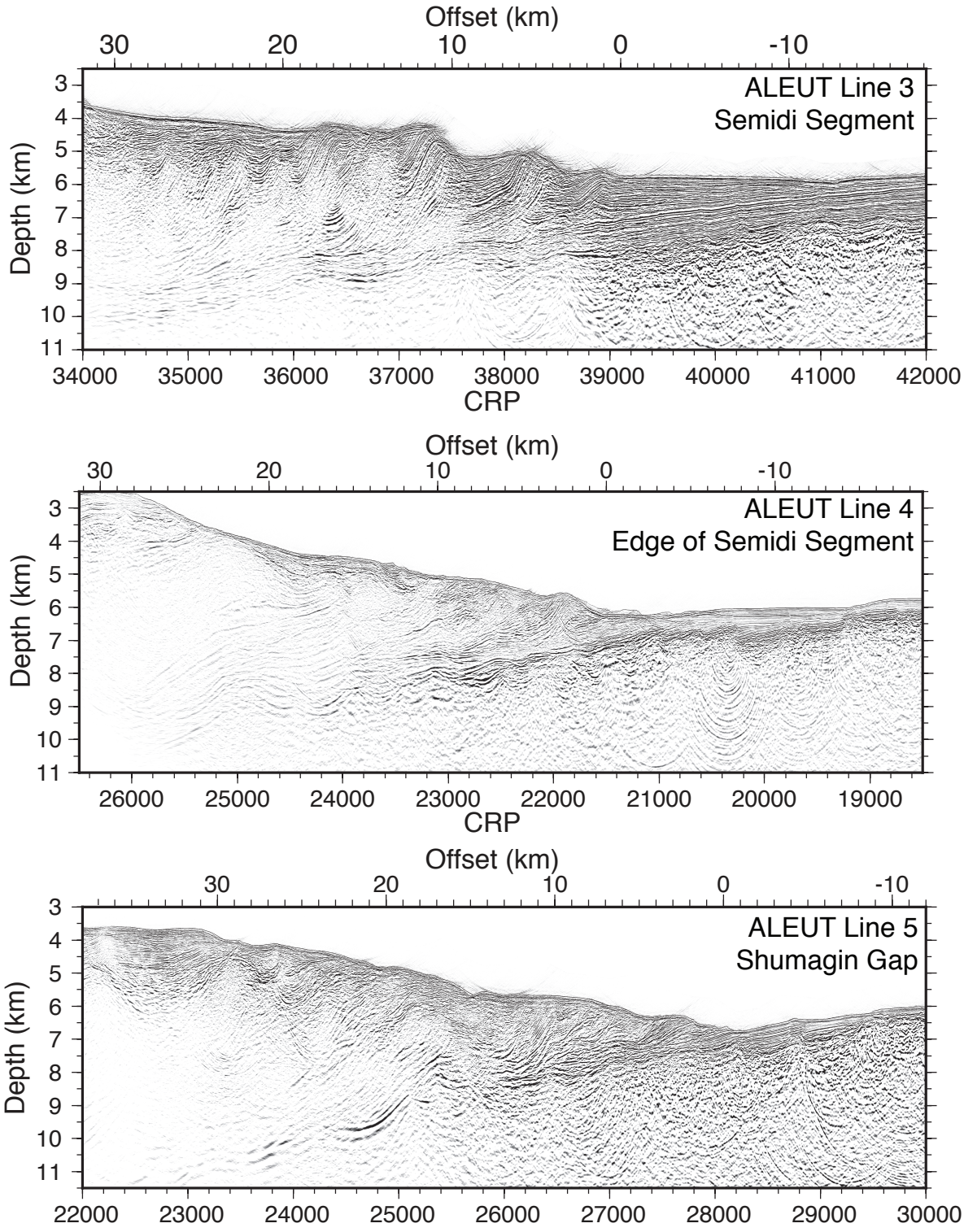

Figure S3, Li et al.

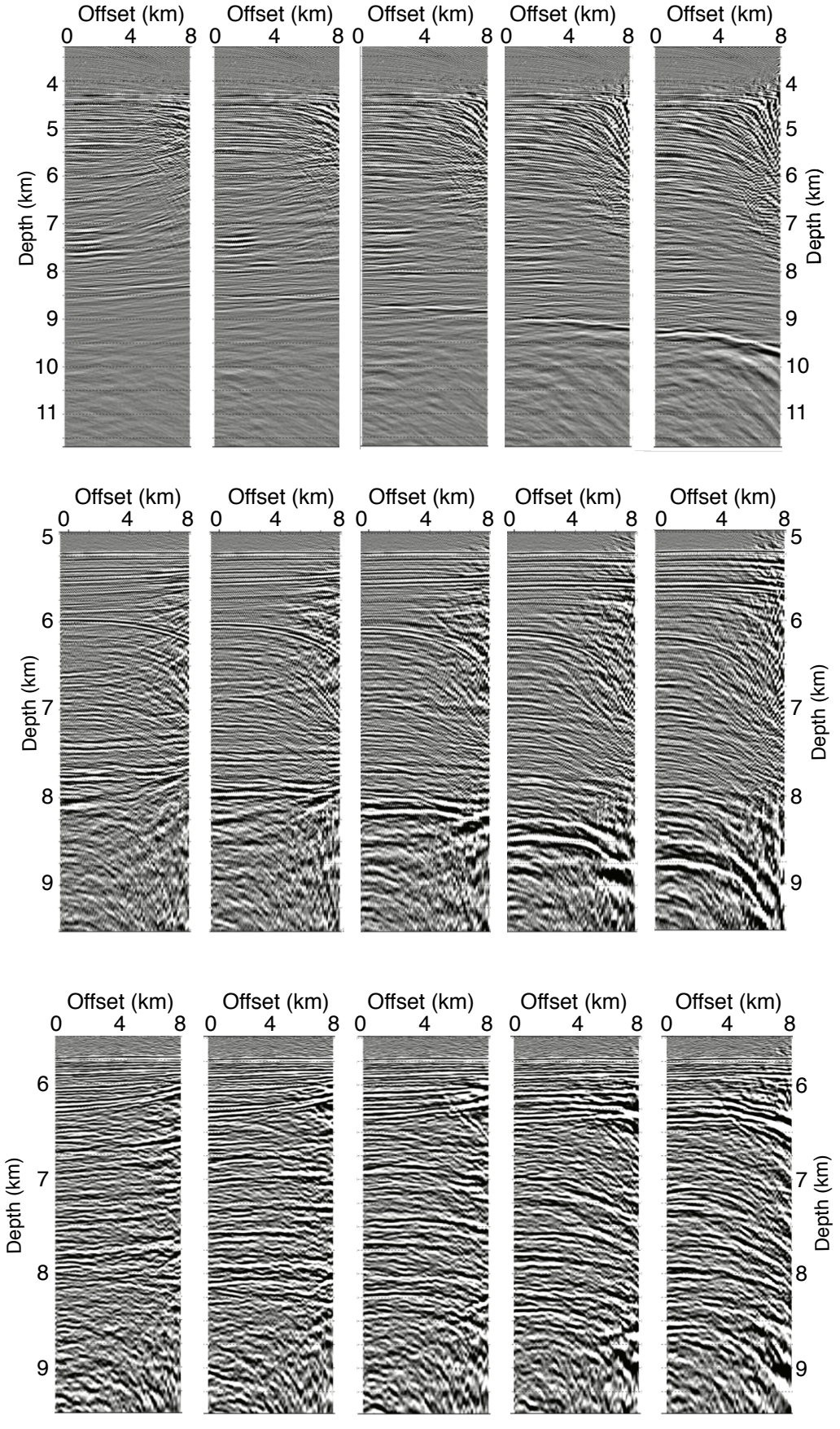

Figure S4, Li et al.

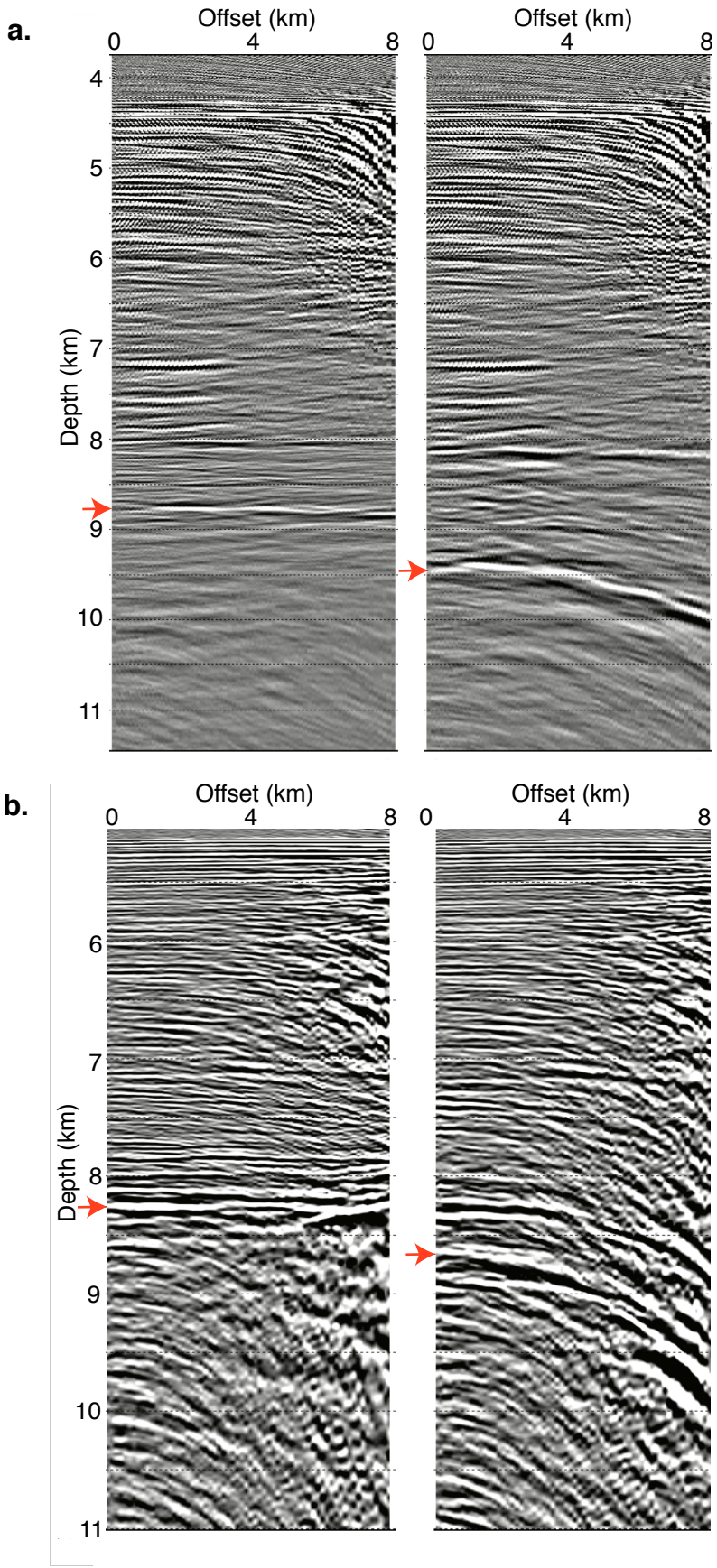

Figure S5, Li et al.

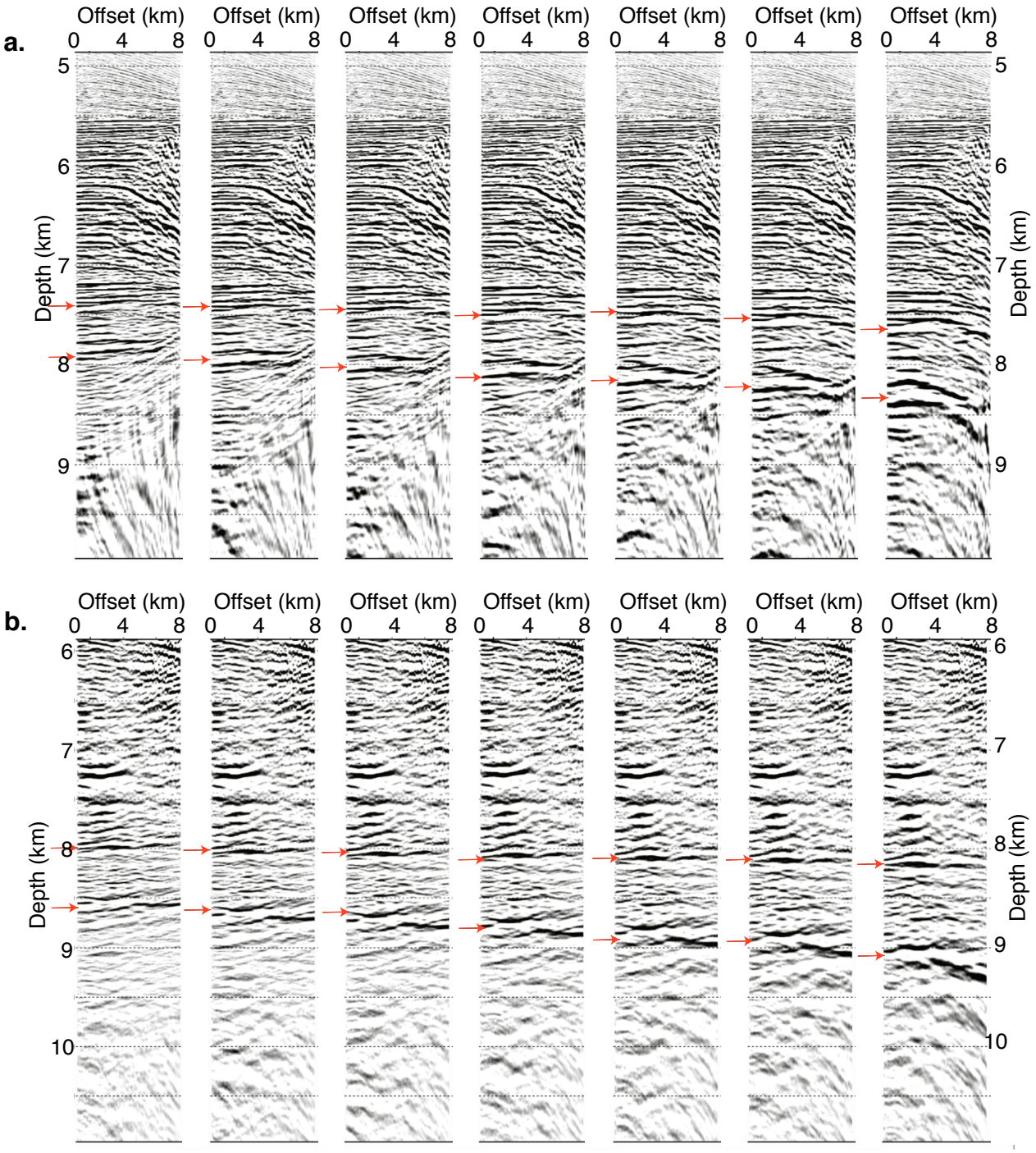

Figure S6, Li et al.

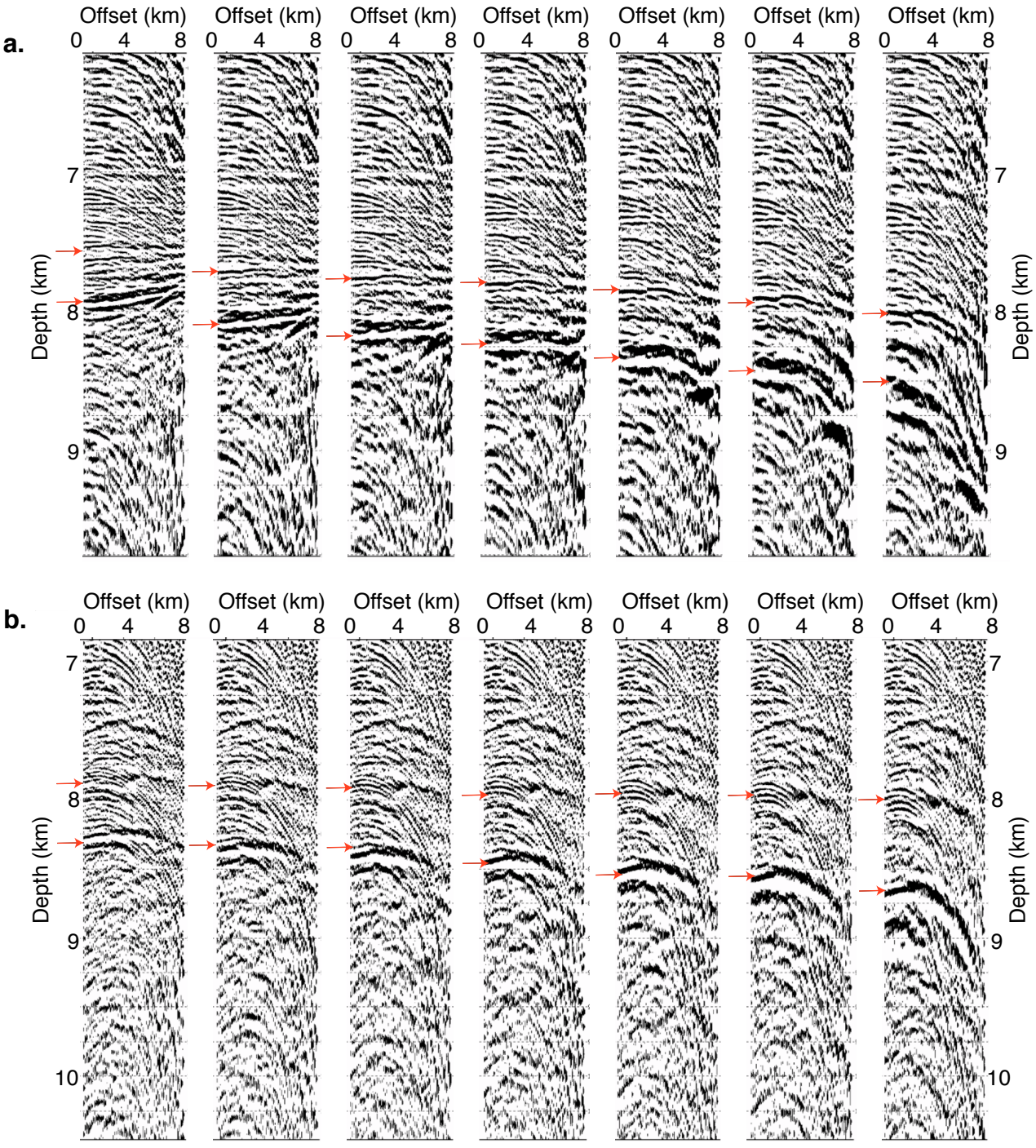

Figure S7, Li et al.

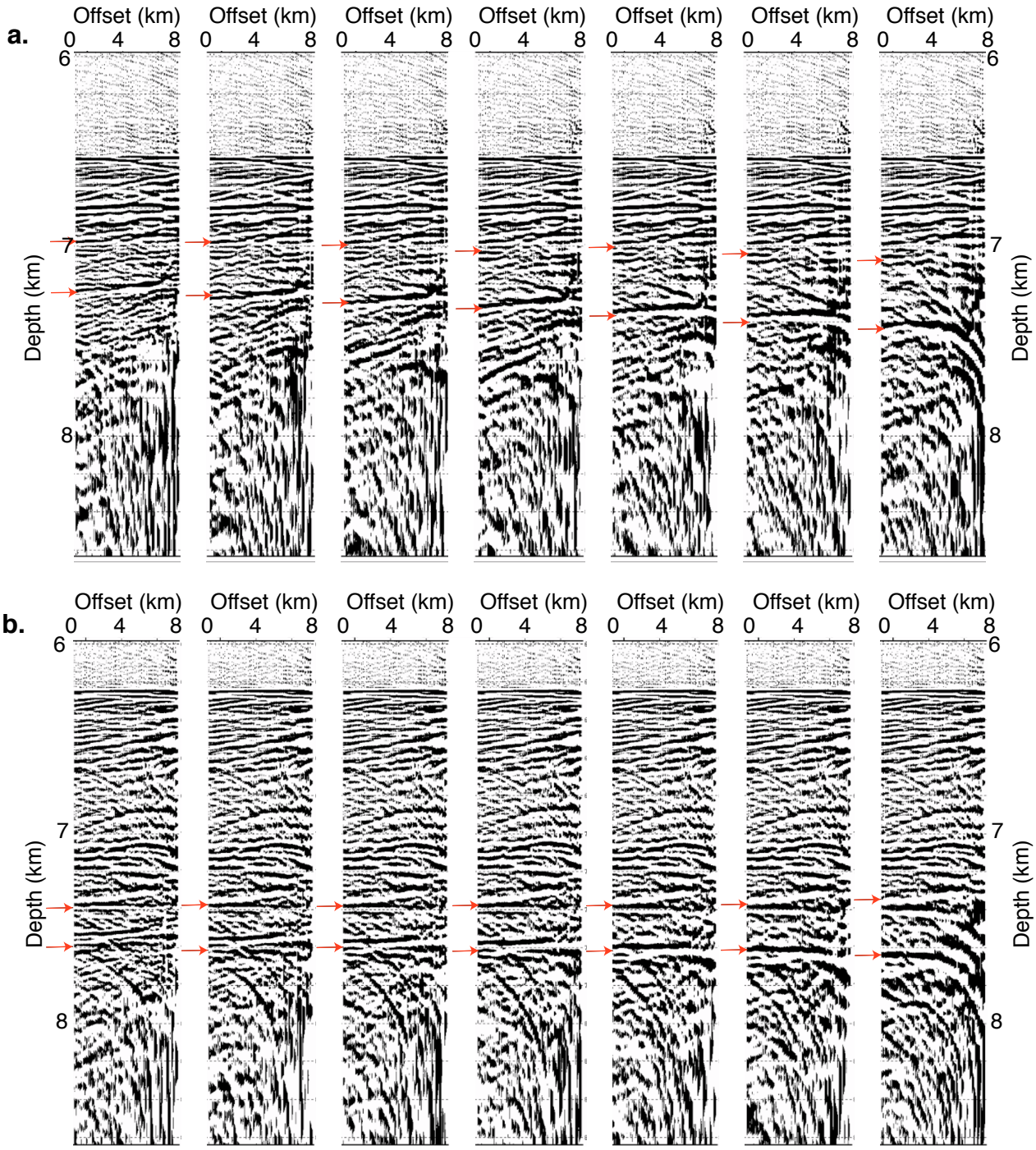

Figure S8, Li et al.